

# I19, the small-molecule single-crystal diffraction beamline at Diamond Light Source

Harriott Nowell,<sup>a</sup> Sarah A. Barnett,<sup>a</sup> Kirsten E. Christensen,<sup>a</sup> Simon J. Teat<sup>b</sup> and David R. Allan<sup>a\*</sup>

<sup>a</sup>Diamond Light Source, Harwell Science and Innovation Campus, Didcot, Oxfordshire OX11 0DE, UK, and

<sup>b</sup>Advanced Light Source, Lawrence Berkeley National Laboratory, 1 Cyclotron Road, Berkeley, CA 94721, USA.

E-mail: david.allan@diamond.ac.uk

The dedicated small-molecule single-crystal X-ray diffraction beamline (I19) at Diamond Light Source has been operational and supporting users for over three years. I19 is a high-flux tunable-wavelength beamline and its key details are described in this article. Much of the work performed on the beamline involves structure determination from small and weakly diffracting crystals. Other experiments that have been supported to date include structural studies at high pressure, studies of metastable species, variable-temperature crystallography, studies involving gas exchange in porous materials and structural characterizations that require analysis of the diffuse scattering between Bragg reflections. A range of sample environments to facilitate crystallographic studies under non-ambient conditions are available as well as a number of options for automation. An indication of the scope of the science carried out on the beamline is provided by the range of highlights selected for this paper.

© 2012 International Union of Crystallography  
Printed in Singapore – all rights reserved

**Keywords:** small-molecule single-crystal diffraction; chemical crystallography; materials; high-pressure; I19.

## 1. Introduction

Beamline I19 at Diamond Light Source, Oxfordshire, UK, is a dedicated high-flux tunable-wavelength facility for the study of small-molecule systems by single-crystal X-ray diffraction techniques. Single-crystal X-ray diffraction remains the method of choice for determining the structure of a crystalline material. The beamline supports a variety of techniques to not only allow the structure determination of demanding crystalline systems (whether they are structurally complex, have a high degree of structural disorder or produce only very small, highly mosaic and weakly diffracting crystals) but also to allow the structural change of systems to be mapped under the influence of an external effect (high pressure, variable temperature, photo-excitation or the exchange of an incorporated gas). The term 'small molecule' encompasses a broad range of materials: from discrete molecular organic and organometallic species to extended metal-organic frameworks, oxides and minerals. The possible applications covered by such materials are similarly broad including, for example, gas storage, molecular machines, pharmaceutical compounds and optical materials. The scientific remit for the beamline was developed, principally, by members of the chemical crystallography community from the experience that had been gained on stations 9.8 (Cernik *et al.*, 1997) and 16.2 at SRS Daresbury Laboratory. Beamline I19 was designed to maintain and extend the range of science supported by the preceding stations and to also take advantage of the high flux available at a third-generation synchrotron source.

The construction phase of I19 was initiated in January 2007 and the beamline became operational, with first users, from September 2008. Over the intervening period approximately 200 user visits have been

supported, including a modest compliment of industrial access. Funding for the construction of the beamline came from the second phase of Diamond's construction budget. Diamond is funded by the UK government *via* the Science and Technology Facilities Council and the Wellcome Trust; these funding partners contribute in proportion to their shareholdings which are 86% and 14%, respectively. Non-proprietary beam time, assessed by peer-reviewed application, is free at the point of access for UK academics.

## 2. Beamline overview

The beamline is located on a 5 m straight-section of the Diamond Light Source storage ring utilizing an in-vacuum U21 undulator as the source of synchrotron radiation. To minimize the ingress of bremsstrahlung radiation into the beamline front-end and optics hutch, the undulator is canted at an angle of 3 mrad to the ideal straight path of the electrons. The optics hutch is positioned against the synchrotron shield (ratchet) wall and, except for some additional beam-defining slits in the experiments hutches, houses all of the beamline optical components (see Fig. 1 and Table 1). Wavelength selection is achieved using a cryo-cooled double-crystal monochromator (DCM) which is currently equipped with a Si-111 crystal set, although the crystal cage has the capacity to accommodate a second crystal set which can be driven into position using an in-vacuum motorized translation stage within the goniostat. The DCM is designed to select energies in the range 5 keV to 28 keV while maintaining a fixed-exit X-ray beam geometry.

Beam focusing is achieved *via* a pair of bimorph mirrors which independently focus the beam in the vertical and horizontal axes. The

**Table 1**

Beamline details.

Beamline name	I19 small-molecule single-crystal diffraction beamline at Diamond
Source type	In-vacuum U21 undulator
Mirrors	A pair of bimorph mirrors (one vertically focusing, one horizontally focusing)
Monochromator	Double-crystal monochromator with Si 111 cryo-cooled crystals
Energy range (keV)	5 to 28
Wavelength range (Å)	0.44 to 2.48
Flux (photons s <sup>-1</sup> )	2.571 × 10 <sup>12</sup> for approximate Gaussian ~170 μm (h) by 85 μm (v) FWHM defocused beam at 150 mA at λ = 1 Å measured at the first sample position using a calibrated diode
Divergence	82 μrad (h) × 31 μrad (v) for unfocused beam at the first sample position at λ = 0.6889 Å

vertical focusing mirror is placed upstream of the horizontal focusing mirror in a common vacuum vessel. To maximize the footprint of the beam over the lengths of the mirrors, the dimensions of the mirrors have been matched to the divergence of the beam and the 3 mrad incidence angle. The vertically focusing mirror (750 mm) is shorter than the horizontally focusing mirror (1000 mm) as the beam divergence (and hence the beam size) in the vertical (31 μrad) is significantly less than the horizontal beam divergence (82 μrad). Both mirror surfaces have three stripes along their lengths: a central stripe of the bare silicon mirror substrate with stripes of rhodium and platinum coated on either side of this. The mirror stripes provide harmonic rejection capability as, at the 3 mrad grazing-incidence angle, the reflectivity of each stripe is strongly energy dependent with well defined cut-off energies of 10 keV, 22 keV and 28 keV for the silicon, rhodium and platinum stripes, respectively. Each stripe provides harmonic free energy in a specific energy range: *i.e.* 5–10 keV for the silicon stripe; 10–22 keV for the rhodium stripe; and 22–28 keV for the platinum stripe. The focused beam has an approximately Gaussian profile with dimensions of 90 μm horizontally (h) × 60 μm vertically (v) FWHM at the first sample position in experiments hutch 1 (EH1) and 185 μm (h) × 130 μm (v) FWHM at the second sample position in experiments hutch 2 (EH2). The bimorphs are routinely defocused to provide a larger beam size for the majority of experiments [defocused beam size is 170 μm (h) × 85 μm (v) FWHM at the first sample position and 190 μm (h) × 130 μm (v) FWHM at the second sample position] as this provides greater flexibility on sample size (ideally, the entire sample is bathed

in the primary beam). The approximate Gaussian profile is closely maintained after this slight defocusing with minimal structure owing to residual slope error in the mirrors.

The mirrors can be retracted from the beam to allow an unfocused, considerably larger, X-ray beam to reach the first sample position directly off the monochromator. The mirror-out mode is only available in EH1 as the beam displacement between the mirror-in and mirror-out modes is too large to be accommodated by the photon shutter between EH1 and EH2. Although there is a significant decrease in intensity at the sample position, this mode is particularly useful for studies requiring a significantly larger beam size, such as high-pressure experiments where accurate crystal centring is difficult. Despite the lack of harmonic rejection, for selected energies of greater than ~18 keV there is little or no discernable λ/3 contamination in the diffraction data as the undulator source produces very little flux at energies greater than ~50 keV.

The beamline routinely operates at the energy of the Zr *K*-edge (17.998 keV) which equates to λ = 0.6889 Å. This wavelength is close to that of a laboratory Mo *K*α X-ray source (λ = 0.7104 Å), which most of the beamline users are familiar with, and has the advantage that it provides reasonable resolution (~0.7 Å) at one setting of the CCD area detector (for a single sample-to-detector distance and 2θ angle). The fixed-exit geometry of the DCM allows wavelength changes with only a minimum of beamline realignment. However, if a change of mirror stripe is required, the voltages for the mirror piezo power supplies need to be reset to reduce the effect of the differing slope error of each stripe on the beam profile. To provide the highest practicable resolution for extremely detailed work, such as electron density studies, or to increase the number of accessible reflections for high-pressure studies, the reference energy of the Ag *K*-edge (25.514 keV, λ = 0.4859 Å) is used. In our experience, this wavelength, which is on the limit of the range of the beamline optics, has been one of the more requested options from the user community. Longer wavelengths have also been requested, for example at the reference energy of the Fe *K*-edge (7.112 keV, λ = 1.7433 Å), to allow determination of accurate absolute structures for molecular crystals containing light atoms. Although the beamline is most often set up at selected reference wavelengths, the design of the optics does naturally allow for a continuous tuning of energy across the design range and this, coupled with the energy resolution of the monochromator (~10<sup>-4</sup> keV), makes it relatively straightforward to perform anomalous dispersion experiments that require one or more fine energy

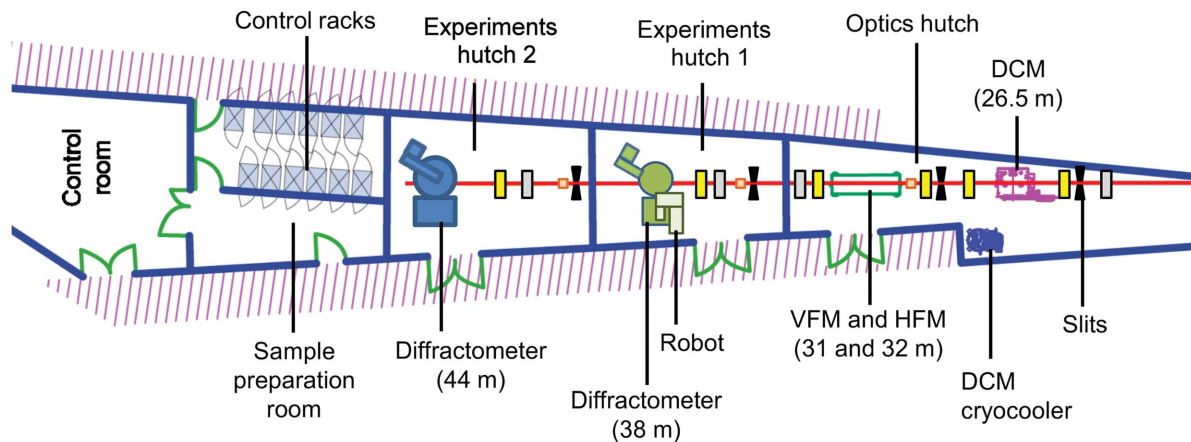


**Figure 1**

Schematic of the beamline layout showing the hutches and positions of the beamline components. Major items are labelled individually: the double-crystal monochromator is shown as DCM while the horizontal focusing mirror and vertical focusing mirror, which share a common vacuum vessel, are indicated as HFM and VFM, respectively. For the other components: the diagnostic units and beam position monitors are indicated by yellow rectangles, grey rectangles represent attenuator units and slits are shown as black wedges. Numbers in parentheses indicate approximate distances, in metres, from the X-ray source while the red line indicates the X-ray path.

**Table 2**

Beamline details for experiments hutch 1 (EH1).

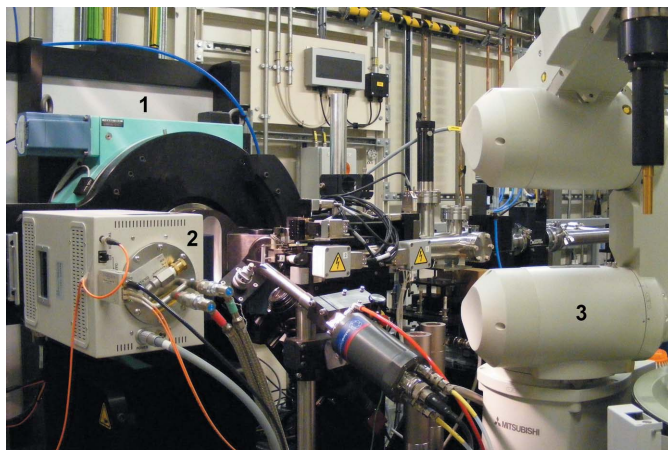
Beam size (uncollimated) ( $\mu\text{m}$ )	Routine defocus to approximate Gaussian $\sim 170$ (h) by 85 (v) FWHM
Goniometer	Four-circle $\kappa$ goniometer ( $\omega$ , $\kappa$ , $\varphi$ , $2\theta$ )
Temperature capability (K)	$\sim 30$ to 500
Sample mounting	Manual or automated
Detector type	CCD
Detector model	Rigaku Saturn 724+
$2\theta$ capabilities	$-30^\circ$ to $65^\circ$ (middle of detector, with a sample-to-detector distance of 60 mm)

changes: for example, to allow different oxidation states for a particular element to be identified.

The beamline is well equipped with diagnostic cameras to monitor the beam position, as indicated on diamond screens, at various key positions both within the optics hutch and the experiments hutches. There are also a range of attenuators that can be used to reduce flux and heat load on the sample and on beamline components. There are a total of five sets of slits used on the beamline to define the beam size (one set is integral to the diffractometer at the first sample position and is, therefore, not shown explicitly in Fig. 1).

The two experiments hutches on I19 are placed in tandem and the instruments they house are designed to support complimentary areas of structural science. The first experiments hutch (EH1), which shares its upstream wall with the optics hutch, is designed principally for high-throughput chemical crystallography studies and has a small, relatively fast, diffractometer (at sample position 1). The diffractometer, manufactured by Crystal Logic, has a four-circle  $\kappa$  geometry and is equipped with a Rigaku Saturn 724+ CCD area detector (see Fig. 2 and Table 2). The sphere of confusion of the goniometer was determined to be  $<10\ \mu\text{m}$  after manufacture and this level of mechanical accuracy is required to ensure that crystals remain well aligned with respect to the beam centre throughout data collection. The  $\varphi$  axis has a standard IUCr goniometer mount containing integral electrical connections for an Oceanering three-axis microglide motorized goniometer head. This is mounted directly to the  $\varphi$  axis of the diffractometer. The diffractometer is mounted on a multi-axis motorized table to allow its accurate alignment to the beam. There is sufficient vertical and lateral travel to displace the diffractometer out of the beam so that additional beam pipes can be fitted when operation is transferred to the second experiments hutch (EH2).

As EH2 is positioned immediately downstream of EH1, it allows users to prepare for more technically difficult experiments in advance

**Figure 2**

The diffractometer set-up in EH1. 1: Crystal Logic goniometer; 2: Rigaku Saturn 724+ detector; 3: Rigaku ACTOR robotic sample changer. Note that a manual goniometer head is mounted.

**Table 3**

Beamline details for experiments hutch 2 (EH2).

Beam size (uncollimated) ( $\mu\text{m}$ )	Routine defocus to approximate Gaussian $\sim 190$ (h) by 130 (v) FWHM
Goniometer	Four-circle $\kappa$ goniometer ( $\omega$ , $\kappa$ , $\varphi$ , $2\theta$ )
Temperature capability (K)	$\sim 4$ to 1200
Sample mounting	Manual
Detector type	CCD
Detector model	Agilent Technologies Atlas
$2\theta$ capabilities	$-30^\circ$ to $120^\circ$ (middle of detector, with a sample-to-detector distance of 60 mm)

of their beam time without effecting the operation of EH1, which can still take beam. With the EH1 diffractometer displaced into a parked position, and with the beam-transport pipe traversing the hutch, beam can then be taken into EH2. As EH2 needs to accommodate a wider variety of experiments, the hutch is relatively large so that peripheral instrumentation can be more easily housed. It is equipped with a significantly larger Newport four-circle goniometer (sample position 2) which can support loads of up to 25 kg on the sample position and, at the time of manufacture, the sphere of confusion was measured to be  $<60\ \mu\text{m}$ . The  $2\theta$ -arm supports an Agilent Technologies Atlas CCD detector with provision made to allow this to be exchanged for a Pilatus 300K photon-counting area detector (see Fig. 3 and Table 3).

The sample preparation room and the room housing the control racks are downstream of EH2, with the control room positioned at the end of the beamline. The layout is shown schematically in Fig. 1.

### 3. Ancillary facilities

#### 3.1. Sample preparation facilities

The beamline has a sample preparation room in addition to a nearby dedicated laboratory. Crystals are usually mounted on MiTeGen micromounts (SPINE standard pin length of 17.6 mm) in oil (or glue for higher-temperature data collections or variable-

**Figure 3**

The diffractometer set-up in EH2. 1: Newport goniometer; 2: Agilent Technologies Atlas detector.

temperature measurements). There is also a corner of EH1 equipped with a bench and a microscope for sample preparation very close to the diffractometer. A glove box and Schlenk lines are available for handling crystals in an oxygen- and water-free environment. There are nitrogen cold-stream devices to facilitate sample preparation at low temperature and for transporting mounted crystals to the diffractometer whilst still under a cold nitrogen gas stream.

### 3.2. Sample environment equipment

Crystals are routinely mounted in an open-flow nitrogen gas cryostat, an Oxford Cryosystems Cryostream Plus, which can provide sample temperatures between 80 K and 500 K and can be operated remotely from the beamline control room. In EH1, for temperatures down to about 30 K it is possible to use the Oxford Cryosystems nHelix open-flow helium device. In EH2 a Cryo Industries of America open-flow helium device is available with a specified base temperature of 4.5 K. For temperatures down to approximately 4 K, an Advanced Research Systems closed-cycle cryostat is available in EH2. Additionally an FMB Oxford hot-gas blower is available for the EH2 diffractometer to allow samples to be heated to approximately 1200 K.

A range of high-pressure experiments have been conducted on the beamline using Merrill–Bassett diamond-anvil cells (Merrill & Bassett, 1974; Moggach *et al.*, 2008). Although diamond-anvil cells are usually brought to the beamline pre-prepared by users for their own experiments, the beamline holds a small stock of cells to allow users who are inexperienced with high-pressure techniques to conduct exploratory studies. The beamline peripheral laboratory has the required high-pressure support equipment, including a ruby fluorescence spectrometer and a gasket hole drill.

The environmental gas cell (Warren *et al.*, 2009) can be used to allow gas exchange in materials containing relatively volatile entrapped molecules, for example in host zeolite framework structures. The cell supports a sufficient vacuum to allow the initial desolvation of the sample crystal for subsequent gas incorporation and it can operate with a range of different gases or gas mixtures.

### 3.3. Excited-state and time-resolved crystallography

Excited-state crystallography of metastable species is facilitated in EH1 with either UV lamps or high-power LEDs arranged in a ring, mounted on the end of the Cryostream nozzle, so that they surround the sample (Brayshaw *et al.*, 2010). These studies are relatively straightforward and require little change from the conventional beamline set-up.

For studies of samples with short-lived excited states, or where the time evolution of the photo-excited phase is of interest, EH2 is equipped with a pulsed laser and an X-ray chopper for pump–probe experiments. The chopper is designed to operate at frequencies between 10 Hz and 10000 Hz (rotary speeds up to 30000 r.p.m.) allowing the study of very short lived species with submillisecond lifetimes.

### 3.4. Automation

EH1 is designed to be a high-throughput facility and the user can choose to automate some aspects of the experimental procedure. EH1 is equipped with a Rigaku ACTOR robotic sample changer which can be operated in a manual mode, where the user controls all key stages of sample transfer and data collection, saving time by avoiding the need to break the hutch interlock between each sample; or fully automatic mode, where sample mounting, centring, screening

(including associated decision making) and subsequent data collection is performed without user intervention. The sample holder associated with the ACTOR robotic sample changer can hold up to 60 samples divided between five standard Rigaku pucks containing up to 12 samples. The standard SPINE length MiTeGen micromount is held *via* a magnetic cryocap (which incorporates a barcode for sample identification) onto the microglide motorized goniometer head. The microglide allows remote manual centring of the crystal, from the control room, or fully automated crystal centring. Automated sample centring is achieved through the use of a software algorithm which uses image recognition to identify the loop of the crystal mount within snapshot images taken through the sample viewing microscope. An iterative sequence of  $\varphi$ -axis rotations and positional corrections are used to accurately centre the loop (at the pre-aligned cross-hair position on the microscope camera). This method of sample centring relies on the crystal being located accurately within the sample loop. There is also a ‘point and click’ procedure for sample centring where the user clicks on the image of the mounted crystal to identify the crystal position; this can be particularly useful when the crystal is not placed accurately within the loop.

### 3.5. Software

The EH1 diffractometer is controlled by Rigaku software, either directly from the *CrystalClear* program or, in fully automatic mode, from the *Director* program (Rigaku, 2010). Although the robotic sample changer can be used in manual mode *via CrystalClear*, the use of *Director* allows experiments to run in an automated manner as the user is able to set up a job involving multiple samples and leave it running unattended. Subsequent data processing is also carried out within the *CrystalClear* suite (Rigaku, 2010), although provision has been made to allow data processing with alternative software packages.

The diffractometer in EH2 can be manually controlled through the Newport *IS4CCD* software (G B C & S, 2011) which also includes a collision model. For data collection with the Atlas CCD detector the experiment run list is set up using *CrysAlisPro* (Agilent Technologies, 2012). The data acquisition is controlled by the Agilent Technologies *IS* software (Agilent Technologies, 2009), and data processing is performed by *CrysAlisPro*. Data collection using the 300K Pilatus detector is performed with the *GDA* software (Gibbons *et al.*, 2012) from Diamond Light Source. Processing of Pilatus data is performed with *XPS* (Kabsch, 2010) and other programs are currently being updated to handle 300K Pilatus data.

## 4. Facility access

There are three access modes described in this section for non-proprietary beam time; applications are made online and are subject to peer review. Beam time for proprietary use is also available and requests should be made *via* the Diamond Industrial Liaison office (industry@diamond.ac.uk).

Direct access is the usual route for beam time on I19. There are two application deadlines each year (usually 1 April and 1 October) with successful applications being awarded beam time in the subsequent allocation period (October–March or April–September, respectively).

Programme access is available to support areas of research that require sustained and guaranteed access to beam time and projects last a maximum of two years. Block Allocation Group (BAG) access is a programme mode of access in which groups of users apply for regular allocations of beam time to be scheduled over a two-year

period. Application deadlines are usually 1 April and 1 October with the two-year period of beam time commencing the subsequent October or April, respectively. The aim of this mode of access is to allow individual academic groups that may have insufficient samples to warrant regular beam time, to join together with other groups and ensure regular synchrotron access.

Rapid access mode is currently allocated at the rate of approximately one day of beam time every other month and is intended for scientifically important and urgent samples. There is a rolling call for applications, and successful applicants are invited to send samples to the facility where the data will be collected by beamline staff.

## 5. Highlights

A number of high-impact scientific results have been published to date using data collected at I19. A significant proportion required the high-flux synchrotron radiation that I19 provides to allow data collection on small or weakly diffracting crystals (for example, Bezzu *et al.*, 2010; Ronson *et al.*, 2011; Sprafke *et al.*, 2011) and two families of materials that come under this category are described in more detail in this section. Other publications have described studies of metastable optically excited species (Philips *et al.*, 2010) and studies of structural change under high pressure (Graham *et al.*, 2011).

There is significant focus at present by supramolecular chemists on the synthesis of rotaxane and catenane materials which are promising candidates for use as molecular machines. Rotaxanes are molecular species consisting of two parts; typically a macrocyclic wheel trapped around a central dumbbell-shaped axle molecule. A recent development that relied upon I19 data for structural characterization involved the introduction of a helical axle molecule to provide a track for the macrocyclic wheel to move along, reversibly, thereby increasing its potential functionality as a molecular machine (see Fig. 4) (Moretto *et al.*, 2009). The inherent nature of these materials means that it is often only possible to grow very small crystals (for example, with at least one crystal dimension being no bigger than 10  $\mu\text{m}$ ) and the high flux available at I19 was essential in this case to collect data of sufficient quality to allow crystal structure solution of this light-atom material. Data quality is also important because refinement of these crystal structures is non-trivial as a result of the large number of atoms in the asymmetric unit and the likely presence of disorder.

Catenanes consist of two or more interlocked macrocycles and recently I19 data was used to solve, for the first time, the crystal structure of a ‘handcuff’ catenane where two covalently linked

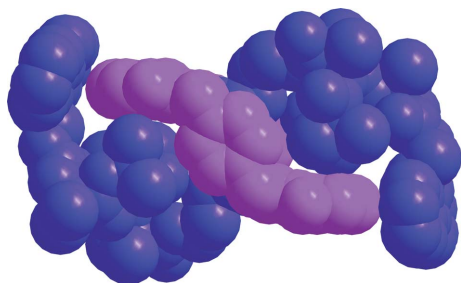


**Figure 4**  
The crystal structure of the rotaxane  $[\text{Fmoc}-(\text{Aib})_n-\text{O}-(\text{CH}_2)_2-\text{NH}]_2-\text{FUM}$ ,  $n = 4$ . The axle is shown in blue and the wheel in purple; H atoms have been omitted for clarity. (Fmoc = 9-fluorenylmethoxycarbonyl; Aib =  $\alpha$ -aminoisobutyric acid; FUM = central fumardiamide unit.)

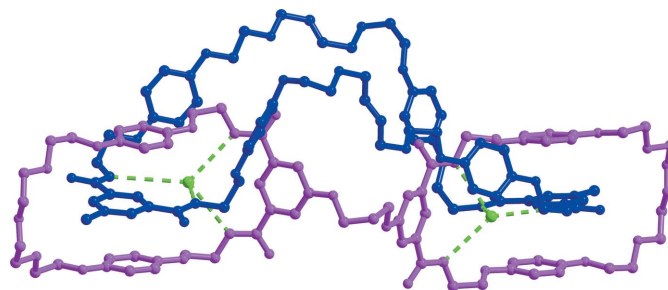


**Figure 5**  
The crystal structure of a ‘handcuff’ catenane. The bis(macrocycle) is shown in purple and the linking macrocycle in blue while the templating chloride ions are green; H atoms have been omitted for clarity.

macrocycles have a third, single, macrocycle passing through the other two rings (see Fig. 5) (Evans *et al.*, 2011).

Metal-organic framework (MOF) materials have also been studied regularly using I19. Applications of MOFs are wide ranging and one area of particularly timely interest is with regard to hydrogen storage. Development of materials with optimal properties for hydrogen storage, such as gas capacity and binding energy, could have a considerable impact on the realisation of the use of hydrogen as an alternative to fossil fuels, for example, in the automotive industry. The large void space in these materials means that they are inherently weakly diffracting. Additionally, the crystals are prone to solvent loss from the channels/pores and can be subject to rapid deterioration under ambient conditions making it essential that the crystals are handled carefully and mounted quickly into the cold stream at the diffractometer. Furthermore, the crystals may be very small, thus exacerbating the weak diffraction and further increasing the requirement for synchrotron radiation. In the study of Yan *et al.* (2010) the structure of one of the MOFs in a series showing particular promise in terms of its high capacity for gas storage was determined on I19 from very weakly diffracting crystals (see Fig. 6). The first crystallographic observation of a photoinduced reaction within a MOF has also been carried out on I19 (Blake *et al.*, 2010), thus illustrating the possibility for MOFs to stabilize photoactive guest moieties and, thereby, facilitating an enhanced understanding of these short-lived species (see Fig. 7).

## 6. Discussion and conclusions

The small-molecule single-crystal beamline at Diamond has supported a wide range of experiments in its first three years of operation. The first experiments hutches (EH1) has been used for a very large number of structure determinations of small and weakly diffracting crystals, for high-pressure crystallography, for variable-temperature structural studies, for excited-state crystallography and for detailed studies of materials with often complex crystal structures. The second experiments hutches (EH2) has been commissioned and initial user experiments have been undertaken including the detailed study of a modulated crystal structure, high-pressure studies and preliminary time-resolved studies.

An upgrade project that is underway is the integration of the Pilatus 300K photon-counting detector into the beamline. This detector has the potential to revolutionize some experiments; it can operate in a shutterless mode so that data collection using continuous scans will be possible, eliminating the need to perform step-scanning, so that data acquisition times will be considerably shorter. The increased dynamic range and zero noise of this detector will reduce

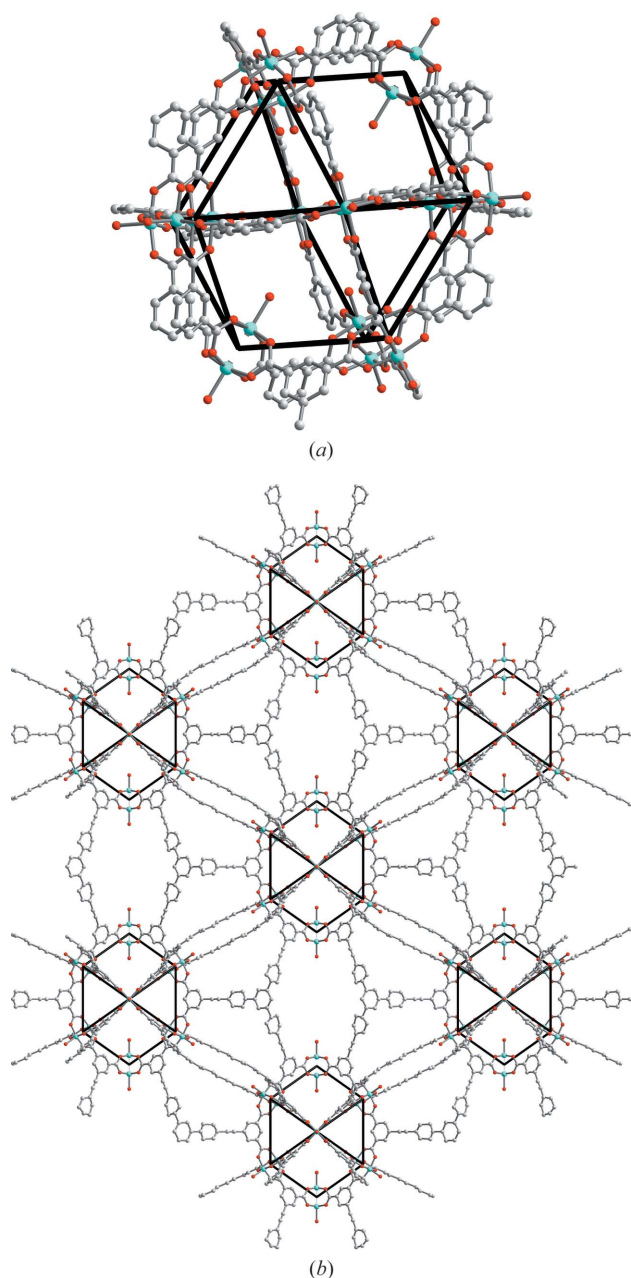


**Figure 6**  
 (a) View of an octahedral cage constructed from 24 isophthalate units and 12  $\{\text{Cu}_2(\text{COO})_4\}$  paddlewheels which serves as a 24-connected node. (b) View of the overall (3,24)-connected network of rht17 topology in NOTT-116. (C, grey; O, red; Cu, blue.)

the problem of simultaneous saturated reflections at low angle and extremely weak high-angle data, which can result in a data set with reduced completeness (as the saturated reflections are rejected at integration) or poor resolution and is caused by the inherent quality of crystals often brought to the beamline.

Development of the protocols for optimal use of a number of the sample environments is underway and, in some cases, the hardware itself is being developed to improve efficiency and ease of use. Optimization of software, hardware and ancillary equipment is expected to be continuous over the coming years while a diverse range of experiments continue to be supported on the beamline. It is anticipated that the most likely revision in the medium term will be

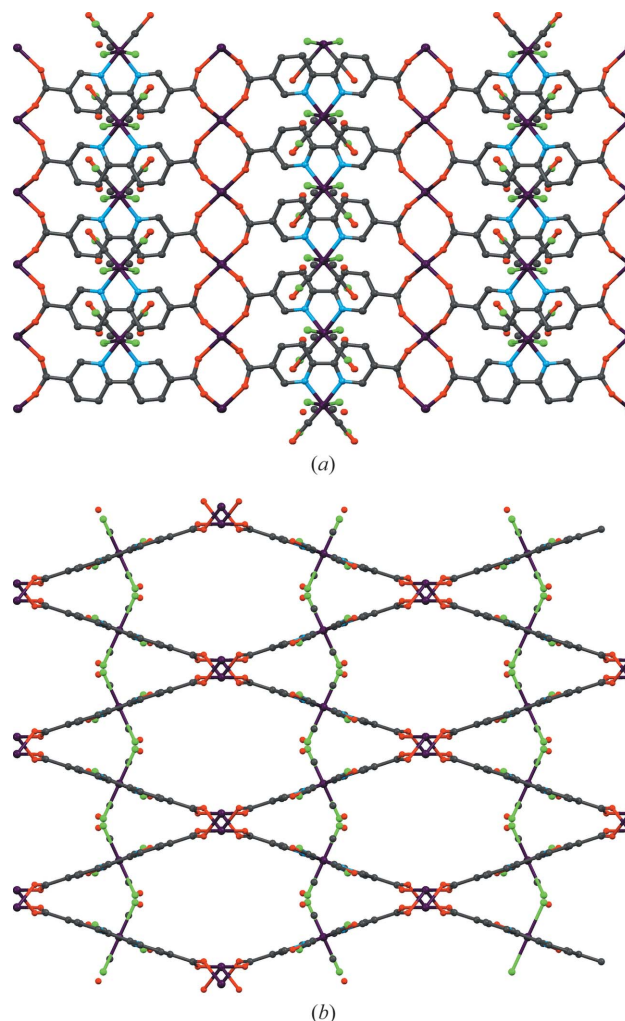


**Figure 7**  
 The crystal structure of  $\{\text{MnCl}_2\text{H}_6\text{N}_2\text{O}_2(\text{DMF})_2\text{Mn}(\text{CO})_3\text{X}\}_\infty$  (X = Br, Cl) viewed down (a) the c-axis and (b) the a-axis. Although the halide CO disorder is shown, H atoms and DMF molecules have been omitted for clarity. (C, grey; O, red; N, blue; Mn, purple; halide, green.)

the implementation of a detector upgrade in EH1, with an accompanying adaptation of the goniometer.

The authors thank all Diamond staff who were involved with the design, construction and commissioning of I19; particularly Vasanthi Nagalingam, Andrew Peach, Matthew Pearson, John Sutter, Stephen Trimmell, Luis Varandas and Adrian Wilcox for their technical expertise. We also thank the beamline working group Paul Raithby, Bill Clegg, Jacqui Cole, Simon Coles, Russell Morris, Sylvain Ravy, John Warren and Claire Wilson for their substantial contribution during the design and construction phase of the beamline.

### References

Agilent Technologies (2009). *IS*. Agilent Technologies, Oxford, UK.  
 Agilent Technologies (2012). *CrysAlisPro*, Version 1.171.35.19. Agilent Technologies, Oxford, UK.  
 Bezzu, C. G., Helliwell, M., Warren, J. E., Allan, D. R. & McKeown, N. B. (2010). *Science*, **327**, 1627–1630.  
 Blake, A. J., Champness, N. R., Easun, T. L., Allan, D. R., Nowell, H., George, M. W., Jia, J. & Sun, X. Z. (2010). *Nat. Chem.* **2**, 688–694.

- Brayshaw, S. K., Knight, J. W., Raithby, P. R., Savarese, T. L., Schiffers, S., Teat, S. J., Warren, J. E. & Warren, M. R. (2010). *J. Appl. Cryst.* **43**, 337–340.
- Cernik, R. J., Clegg, W., Catlow, C. R. A., Bushnell-Wye, G., Flaherty, J. V., Greaves, G. N., Burrows, I., Taylor, D. J., Teat, S. J. & Hamichi, M. (1997). *J. Synchrotron Rad.* **4**, 279–286.
- Evans, N. H., Serpell, C. J. & Beer, P. D. (2011). *Angew. Chem. Int. Ed.* **50**, 2507–2510.
- G, B, C, & S (2011). *IS4CCD*, Version 3.00-C. G B C and S, Brie Comte Robert, France.
- Gibbons, E. P., Heron, M. T. & Rees, N. P. (2012). *13th International Conference on Accelerator and Large Experimental Physics Control Systems (ICALPECS 2011)*, 10–14 October 2011, Grenoble, France.
- Graham, A. J., Allan, D. R., Muszkiewicz, A., Morrison, C. A. & Moggach, S. A. (2011). *Angew. Chem. Int. Ed.* **50**, 11138–11141.
- Kabsch, W. (2010). *Acta Cryst.* **D66**, 125–132.
- Merrill, L. & Bassett, W. A. (1974). *Rev. Sci. Instrum.* **45**, 290–294.
- Moggach, S. A., Allan, D. R., Parsons, S. & Warren, J. E. (2008). *J. Appl. Cryst.* **41**, 249–251.
- Moretto, A., Menegazzo, I., Crisma, M., Shotton, E. J., Nowell, H., Mammi, S. & Toniolo, C. (2009). *Angew. Chem. Int. Ed.* **48**, 8986–8989.
- Philips, A., Cole, J., d'Almeida, T. & Low, K. S. (2010). *Phys. Rev. B*, **82**, 155118.
- Rigaku (2010). *CrystalClear-SM Expert*, Version 2.0 r5. Rigaku Americas, The Woodlands, Texas, USA.
- Ronson, T. K., Nowell, H., Westcott, A. & Hardie, M. J. (2011). *Chem. Commun.* **47**, 176–178.
- Sprafke, J. K. *et al.* (2011). *J. Am. Chem. Soc.* **133**, 17262–17273.
- Warren, J. E., Pritchard, R. G., Abram, D., Davies, H. M., Savarese, T. L., Cash, R. J., Raithby, P. R., Morris, R., Jones, R. H. & Teat, S. J. (2009). *J. Appl. Cryst.* **42**, 457–460.
- Yan, Y., Telepeni, I., Yang, S., Lin, X., Kockelmann, W., Dailly, A., Blake, A. J., Lewis, W., Walker, G. S., Allan, D. R., Barnett, S. A., Champness, N. R. & Schröder, M. (2010). *J. Am. Chem. Soc.* **132**, 4092–4094.